Thermal and magnetic properties of the low-temperature antiferromagnet $Ce_4Pt_{12}Sn_{25}$

Nobuyuki Kurita,[1] Han-Oh Lee,[1,2] Yoshi Tokiwa,[1] Corneliu F. Miclea,[1] Eric D. Bauer,[1] Filip Ronning,[1] J. D. Thompson,[1] Zachary Fisk,[2] Pei-Chun Ho,[3,4] M. Brian Maple,[3] Pinaki Sengupta,[1,5] Ilya Vekhter,[6] and Roman Movshovich[1]

[1]*Los Alamos National Laboratory, Los Alamos, New Mexico 87545, USA*

[2]*University of California, Irvine, California 92697, USA*

[3]*Department of Physics, University of California–San Diego , La Jolla, California 92093, USA*

[4]*Department of Physics, California State University–Fresno, Fresno, California 93740, USA*

[5]*School of Physical and Mathematical Sciences, Nanyang Technological University, 21 Nanyang Link, Singapore 637371*

[6]*Department of Physics & Astronomy, Louisiana State University, Baton Rouge, Louisiana 70803, USA*

(Received 1 September 2010; published 19 November 2010)

We report specific heat (C) and magnetization (M) of single crystalline $Ce_4Pt_{12}Sn_{25}$ at temperature down to ~50 mK and in fields up to 3 T. C/T exhibits a sharp anomaly at 180 mK, with a large $\Delta C/T \sim 30$ J/mol Ce K^2, which, together with the corresponding cusplike magnetization anomaly, indicates an antiferromagnetic (AFM) ground state with a Néel temperature $T_N=180$ m K. Numerical calculations based on a Heisenberg model reproduce both zero-field C and M data, thus placing $Ce_4Pt_{12}Sn_{25}$ in the weak exchange coupling $J<J_c$ limit of the Doniach diagram, with a very small Kondo scale $T_K \ll T_N$. Magnetic field suppresses the AFM state at $H^* \approx 0.7$ T, much more effectively than expected from the Heisenberg model, indicating additional effects possibly due to frustration or residual Kondo screening.

DOI: 10.1103/PhysRevB.82.174426 PACS number(s): 75.20.Hr, 71.27.+a, 71.70.Ch, 75.50.Ee

I. INTRODUCTION

Compounds with elements containing $4f$ and $5f$ electrons, such as Ce, Yb, and U, have been subjects of intense research over the past several decades. Rich physics displayed within this class of materials can be directly attributed to the interaction of f electrons with conduction electrons, which leads to, among other aspects, competing ground states. Heavy electron ground states are often thought to be a consequence of the Kondo exchange interaction, J, between the f and conduction c electrons.[1] At each site this interaction favors the formation of the local f-c Kondo singlet and leads to large effective masses of the charge carriers. The same f-c exchange term also leads to the Ruderman-Kittel-Kasuya-Yosida (RKKY) (Refs. 2–4) magnetic coupling between the f ions mediated by the polarization of the conduction electrons. The latter effect generally favors long-range magnetic [often antiferromagnetic (AFM)] ground state of the f ions.

Competition between the Kondo effect and RKKY interaction was originally addressed by Doniach in the one-dimensional-chain model,[5,6] for different values of the AFM Kondo coupling. At low J the long-range AFM ground state of f ions is stabilized. With increasing J the AFM ground state is suppressed, yielding to a Kondo screened state beyond a critical value, J_c. Pressure can be effective in changing on-site J by increasing the overlap between the f and c states. A number of compounds were discovered that are located in the vicinity of the $T=0$ phase transition between the heavy fermion (HF) and AFM ground states, often manifested as a quantum critical point (QCP). Non-Fermi-liquid (NFL) behavior displayed by compounds in the vicinity of QCPs, such as the divergent Sommerfeld coefficient, $C/T \propto -\ln T$ behavior found in $CeCu_{5.9}Au_{0.1}$,[7] $YbRh_2Si_2$,[8] and $CeCoIn_5$,[9,10] linear, in temperature, resistivity, and other anomalous properties, provides additional impetus to research on competition between HF physics and magnetism. The NFL behavior in d- and f-electron systems is reviewed, for example, in Refs. 11 and 12.

There have been a number of theoretical attempts to model such systems using the periodic Anderson model[13] and Kondo lattice model.[14] A mean-field model of the Kondo lattice including the nearest-neighbor magnetic interaction[15] yields a reduction in the Kondo temperature, T_K, at $J>J_c$ compared to its value for a single impurity. This result emphasizes the importance of the RKKY coupling even when the system is in the Kondo (HF) ground state. On the other hand, for $J<J_c$, on the AFM side of the QCP in the Doniach analysis, a mean-field renormalization group approach[16] provided a good agreement between theory and the experimental results[17] on the pressure-tuned AFM transition temperatures in a series of CeT_2Si_2 (T=Ru, Rh, and Pd) compounds. However, the interplay between the Kondo and RKKY interactions in this regime is not yet fully understood,[18] and additional work, both theoretical and experimental, is needed. In this paper we provide an example of a compound which orders magnetically at low temperature, in the regime where previously studied compounds display dominant Kondo screening.

An alternative to the pressure route of tuning the relative strength of the Kondo screening and AFM coupling is via synthesis, i.e., crystallographic structure of the compounds. For a specific value of the on-site f-c exchange constant J one expects the RKKY interaction, which decays as a power law in $k_F r$, where k_F is the Fermi momentum and r is the distance between the magnetic ions, to become weaker the further the f atoms are separated from one another. As a result, the Kondo screening should commonly win over magnetic ordering in such dilute systems. It would therefore be particularly interesting to explore the f electron bearing compounds with large f-f nearest-neighbor distances. Several stoichiometric dilute f-electron compounds have been useful in this regard. Ce-based filled skutterudites CeT_4X_{12} (T=Fe, Ru, Os; X=P, As, Sb, $d_{Ce\text{-}Ce} \sim 7$ Å) form one of these families, with most members semiconducting with the gap size that correlates with the lattice constant.[19] Another example is a family of Yb-based HF compounds YbA_2Zn_{20} (A=Fe, Co,

Ru, Rh, Os, Ir, $d_{\text{Yb-Yb}} \sim 6$ Å),[20–22] where the Kondo physics appears to dominate the RKKY interaction, in accord with the simple argument above.

The approach of synthesizing compounds with large f-f nearest-neighbor distance also turned out to be useful in the studies of electronic correlations in uranium compounds. Large U-U distance $d_{\text{U-U}} \sim 6$ Å in UM_2Zn_{20} (M=Co,Rh) family of materials reduces the overlap between the 5f-electron wave functions, allowing for observation of sharp crystal electric fields (CEFs), a situation very rare in U compounds.[23] At the same time, this U-U separation resulted in a good description of the system within a Kondo limit of the Anderson model, i.e., UM_2Zn_{20} compounds are found to be well on the Kondo side of the QCP, similar to the YbT_2Zn_{20} case above, and again in accord with expectations above.

$Ce_4Pt_{12}Sn_{25}$ presents another example of a metallic 4f-dilute Ce-based system,[24] with Ce-Ce interatomic distance $d_{\text{Ce-Ce}}$=6.14 Å. It therefore appears to be a good candidate to continue exploration of correlated electron physics in f-electron systems, and, in particular, the competition between the RKKY interaction and Kondo screening. $Ce_4Pt_{12}Sn_{25}$ is a cubic compound lacking fourfold point symmetry with three inequivalent Sn sites. Recently, we succeeded in growing single crystals of $Ce_4Pt_{12}Sn_{25}$ with relatively large physical dimensions (up to $\sim 5\times5\times5$ mm^3).[25] Previous specific-heat, resistivity, and ac-susceptibility measurements uncovered a phase transition at 0.18 K.[25] However, the origin of the transition was not identified. In this paper, we report the low-temperature specific-heat (C) and magnetization (M) measurements in magnetic field. From the cusp and the field dependence in $M(T)$, which corresponds to the specific-heat anomaly, we conclude that $Ce_4Pt_{12}Sn_{25}$ is an antiferromagnet with T_N=0.18 K in zero field. Evolution of C/T and M with magnetic field indicates disappearance of AFM ordering and subsequent splitting of an f-electron ground-state doublet. We find that the signatures of the magnetic transition are reasonably close to those described by a spin-1/2 Heisenberg model, albeit with notable differences, see below. This suggests that even for the large distance between the neighboring 4f ions the RKKY interaction plays a very significant, or even dominant, role.

II. EXPERIMENTAL DETAILS

Single crystals of $Ce_4Pt_{12}Sn_{25}$ were grown by Sn self-flux method. The details of the sample growth and the physical properties are described in Ref. 25. Specific heat was measured in a SHE dilution refrigerator with 9 T superconducting magnet by means of a quasiadiabatic heat-pulse method with a RuO_2 thermometer. The low-temperature high-resolution dc magnetization measurements were performed in a commercial Oxford Kelvinox dilution refrigerator with 12–14 T superconducting magnet. We used a capacitive Faraday magnetometer cell with applied field gradient of 10 T/m. The principle of the magnetization measurement is described in Ref. 26. By comparing the data from a commercial magnetic property measurement system (MPMS; Quantum Design) up to 7 T and down to 2 K with that obtained with capacitive method in the same field and temperature range, we are able to determine the absolute value of the magnetization. We used three samples from different batches labeled as samples #1 (7.18 mg), #2 (2.58 mg), and #3 (3.70 mg) in the figures in this paper for specific-heat measurements. We used a sample weighing 4.63 mg for magnetization measurements.

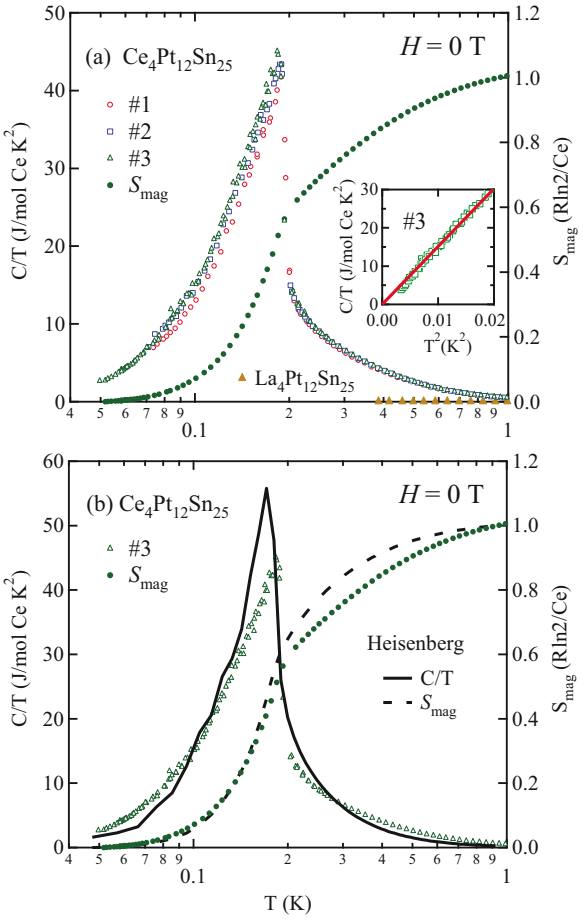

FIG. 1. (Color online) (a) Temperature dependence of C/T of $Ce_4Pt_{12}Sn_{25}$ for samples #1, #2, and #3, and of the La-analog $La_4Pt_{12}Sn_{25}$ in zero field. Solid dots represent the temperature dependence of magnetic entropy S_{mag} in units of R ln 2. Inset: C/T vs T^2 at low temperature. The solid line is a linear least-squared fit to the data. (b) △-C/T and ●-S of $Ce_4Pt_{12}Sn_{25}$ (sample #3). Solid and dashed lines represent specific heat and entropy, respectively, from the Heisenberg model calculations described in the text.

III. RESULTS AND DISCUSSIONS

A. Specific heat

Figure 1 shows the temperature dependence of C/T of $Ce_4Pt_{12}Sn_{25}$ (50 mK–3 K) for samples #1, #2, and #3, and that of a nonmagnetic analog $La_4Pt_{12}Sn_{25}$ (0.4–3 K) in zero field. C/T of $La_4Pt_{12}Sn_{25}$ is negligible compared to that of $Ce_4Pt_{12}Sn_{25}$ in the investigated temperature range. Therefore, the obtained specific heat of $Ce_4Pt_{12}Sn_{25}$ can be regarded as purely of magnetic origin C_{mag}. With temperature decreasing from 3 K, C/T monotonically increases down to 0.18 K, at

which point it exhibits a sharp anomaly with the magnitude of the jump $\Delta C/T \sim 30$ J/mol Ce K^2. From magnetization measurements we identify this anomaly as due to AFM ordering, as discussed below. In addition, low-temperature T^2 variation in C/T, shown in the inset, is consistent with the spin-wave contribution in the AFM state. Solid circles represents the temperature dependence of the magnetic entropy $S_{\rm mag}(T)$ of $Ce_4Pt_{12}Sn_{25}$,

$$S_{\rm mag}(T) = \int_0^T \frac{C_{\rm mag}}{T} dT. \quad (1)$$

Entropy gain is $\approx 0.5R \ln 2$ at T_N and reaches the value of $1.0R \ln 2$ at 3 K. This indicates that the CEF ground state of Ce^{3+} in $Ce_4Pt_{12}Sn_{25}$ is a Γ_7 doublet. One remarkable feature of the specific heat of $Ce_4Pt_{12}Sn_{25}$ is the long tail above T_N. As we show below, a substantial part of this tail is due to quantum fluctuations of f-electron spins above T_N. However, from our analysis it is likely that other processes, such as residual Kondo screening, or frustration of spin-spin interactions play some role. Similar C/T behavior was reported in the structurally frustrated system Yb_2Pt_2Pb,[27] for example.

To elucidate the origin of this behavior we performed quantum Monte Carlo simulations of the spin-1/2 three-dimensional Heisenberg model in zero and applied magnetic field. The exchange interaction was fixed to have the AFM ordering temperature of $T_N=0.18$ K for $H=0$ while the g factor of the spins was determined from the saturation magnetization at high fields (see below). The results for zero-field specific heat and entropy are displayed in Fig. 1 as solid and dashed curves, respectively. The agreement between the model calculations and experimental data is rather good. In particular, the behavior of the entropy below T_N is very similar, and the entropy at T_N for model calculations is about $0.55R \ln 2$, about 10% larger than the experimental value. The most notable difference is that experimental entropy is lower than the calculated values above the transition, indicating that some degrees of freedom remain "locked." This discrepancy is also seen from the somewhat longer tail of the measured specific heat in Fig. 1(b) relative to the Heisenberg model. Such contribution may still be due to remnant Kondo physics. Recall that the distance between Ce ions is large, and therefore RKKY exchange, and correspondingly the critical J_c, is reduced. In the framework of Doniach phase diagram, the only situation when RKKY interaction can still dominate the Kondo coupling is when the bare exchange J is very small. $Ce_4Pt_{12}Sn_{25}$ is therefore in the low $J<J_c$ limit of the Doniach phase diagram, and the system orders magnetically below $T_N=0.18$ K. Note that Ce-based skutterudite compounds and YbA_2Zn_{20}, whose Ce-Ce and Yb-Yb distances are similar to that in $Ce_4Pt_{12}Sn_{25}$, do not show magnetic ordering, and are in the $J>J_c$ Kondo limit. It should also be noted that there is no significant sample dependence for different samples #1, #2, and #3, with respect to the ordering temperature, the magnitude of the anomaly in C/T, and its width.

Figure 2 shows C/T for magnetic field (a) $0 \le B \le 0.65$ T and (b) $0.65 \le B \le 3.0$ T. As shown in Fig. 2(a), the steep jump in C/T associated with AFM ordering is

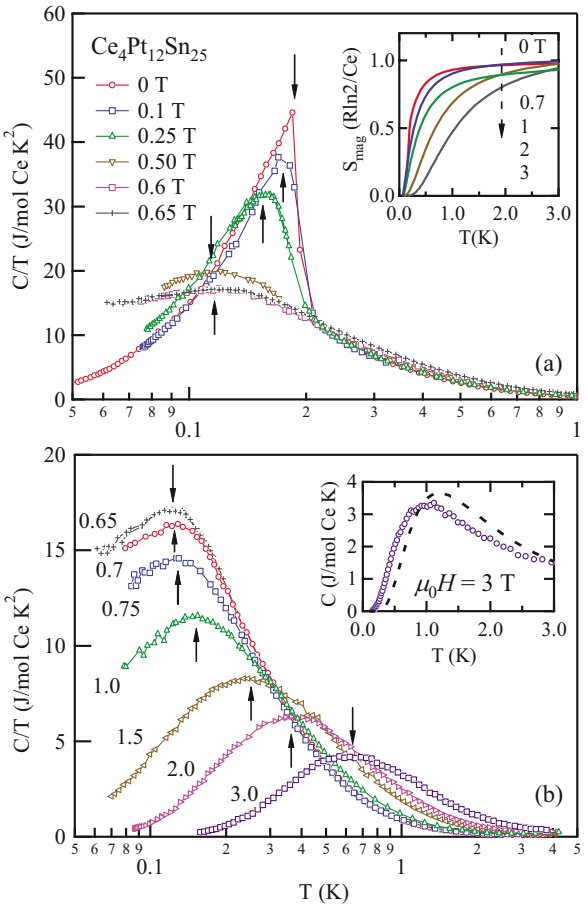

FIG. 2. (Color online) Temperature dependence of C/T of $Ce_4Pt_{12}Sn_{25}$ in the magnetic fields, (a) 0–0.65 T and (b) 0.6–3 T. The arrows indicate the temperature where C/T has maximum. The inset (a): $S_{\rm mag}(T)$ in several fields up to 3 T. The inset (b): $C(T)$ at $B=3$ T. The dashed curve is obtained based on the CEF calculation defined in the text.

quickly suppressed, and $T_{\rm max}$, where C/T has its maximum value, gradually shifts to lower temperature, as indicated by arrows. On the other hand, Fig. 2(b) shows that with further increase in magnetic fields, $T_{\rm max}$ shifts to higher temperature while the peak height is continuously suppressed. This behavior can be understood as follows: In the low-field region the reduction in $T_{\rm max}$ is ascribed to the suppression of the AFM ordering with field ($T_{\rm max} \approx T_N$). Around 0.7 T, the feature associated with the AFM order is suppressed entirely. Further increase in magnetic field increases Zeeman splitting of the CEF doublet ground state (see below), leading to a Schottky anomaly in specific heat with rising $T_{\rm max}$. Similar behavior has been observed in a number of other Ce compounds, e.g., $CeCu_{5.9}Au_{0.1}$,[28] $CeCu_2Si_2$,[29] and $(La,Ce)Al_2$.[29,30] As seen in the inset of Fig. 2(a), $S_{\rm mag}$ reaches $1.0R \ln 2$ independently of applied fields up to 3 T, although the ground state and the shape of the specific-heat anomaly both vary strongly with applied field, reflecting a twofold degeneracy of the CEF doublet.

At high magnetic fields, far exceeding the Heisenberg exchange coupling, we can obtain the approximate behavior of $Ce_4Pt_{12}Sn_{25}$ based on the CEF level scheme. To avoid complication in parametrizing, we assume that a cubic point

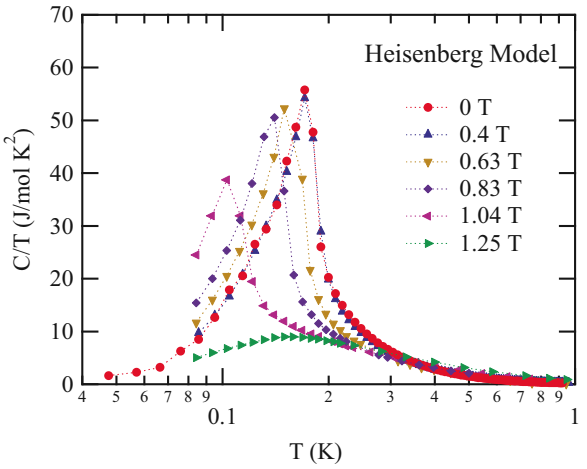

FIG. 3. (Color online) Sommerfeld coefficient $\gamma = C/T$ calculated in the nearest-neighbor Heisenberg model as function of T at low and intermediate fields.

symmetry of Ce ions in $Ce_4Pt_{12}Sn_{25}$ is O_h and the CEF Hamiltonian H_{CEF} can be reduced to the following formula:[31]

$$H_{CEF} = \sum_{m,n} B_n^m O_n^m = B_4^0 (O_4^0 + 5O_4^4), \tag{2}$$

where B_n^m and O_n^m are the CEF parameters and the Stevens operators,[32,33] respectively. The total Hamiltonian H and specific heat C of CEF levels in external magnetic fields is then given by the following expression:

$$H = H_{CEF} - g_J \mu_B \boldsymbol{J} \cdot \boldsymbol{H}, \tag{3}$$

$$C = \frac{\partial}{\partial T} \frac{1}{Z} \sum_n E_n e^{-\beta E_n}. \tag{4}$$

Here, g_J is the Lande g factor, E_n and $|n\rangle$ are the nth eigenvalue and eigenfunction, respectively, $Z = \Sigma_n e^{-\beta E_n}$, $\beta = 1/k_B T$, and k_B is the Boltzmann constant. We assume that the ground state is a Γ_7 doublet. $B_4^0 = 0.5$ K then corresponds to the CEF splitting between Γ_7 and the first excited state $\Delta \approx 200$ K, which can be inferred from $S_{mag}(T)$ and resistivity data,[25] respectively. As shown in the inset of Fig. 2(b), the calculated specific-heat anomaly at 3 T (dotted curve) closely reproduces experimental results, supporting the CEF scheme suggested above.

Quick suppression of the AFM specific-heat anomaly in the low-field regime, displayed in Fig. 2(a), and particularly the broadening of the anomaly with magnetic field, makes precise identification of $T_N(H)$ difficult. Encouraged by the success of our Heisenberg model calculations in zero field, we performed calculations for this model in finite field, with the goal to aid in identification of T_N in experimental data. Figure 3 displays the results of these calculations. There are striking differences between the model and experimental data. In the Heisenberg model the specific-heat anomaly at the AFM phase transition remains sharp, and persists to high fields over 1 T while the experimentally observed anomaly is washed out already by 0.5 T. There are a number of possible reasons for this discrepancy. A Heisenberg model is often used to describe insulating compounds, with coupling J independent of the magnetic field. In our case the magnetic coupling is mediated by the conduction electrons, with a potential for a field-dependent magnetic coupling. The effect of the next-nearest-neighbor interaction, with accompanying effects of possible frustration, is also neglected in the present calculations. Among other complications is a possible proximity to a HF (Kondo) ground state. Our results point to a number of fruitful future theoretical inquiries, such as field-dependent RKKY interaction, or including frustration within the Heisenberg model due to next-nearest-neighbor interactions, and its response to magnetic field.

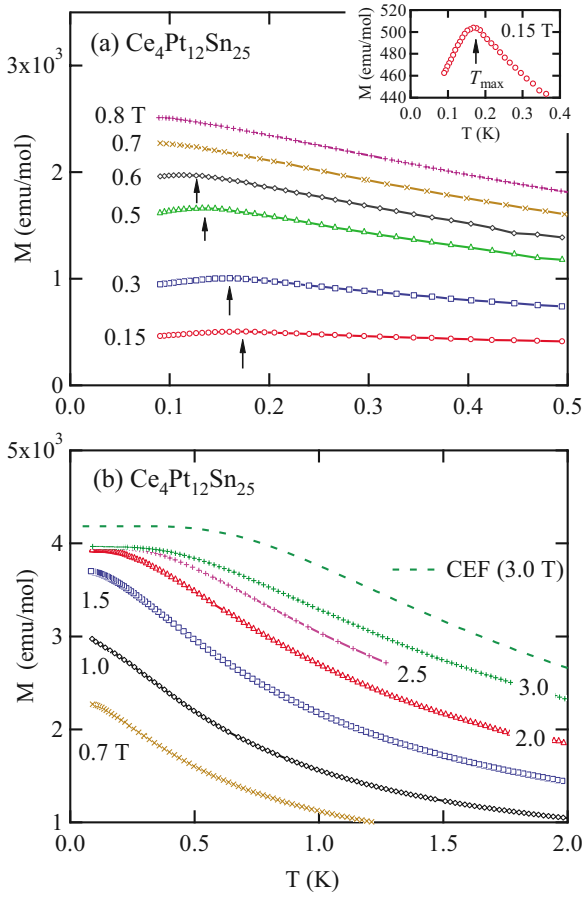

FIG. 4. (Color online) Temperature dependence of magnetization $M(T)$ of $Ce_4Pt_{12}Sn_{25}$ in several fields (a) 0–0.8 T and (b) 0.7–3 T. The arrows in (a) indicate T_{max} where $M(T)$ exhibits maximum as displayed in the inset of (a). The dashed curve in (b) represents a calculated result at 3 T based on the CEF effect (see text).

B. Magnetization

Figure 4 shows temperature dependence of the magnetization $M(T)$ for $T \ll 2$ K in fields (a) up to 0.8 T and (b) between 0.7 and 3.0 T. The low-temperature data connect well to the higher temperature data obtained using a MPMS (not shown). The cusp in M vs T in the low-field region identified by arrows in Fig. 4(a) reflects the AFM ordering phase transition. As an example, the inset of Fig. 4(a), shows $M(T)$ at 0.15 T, on expanded scale, which exhibits a clear

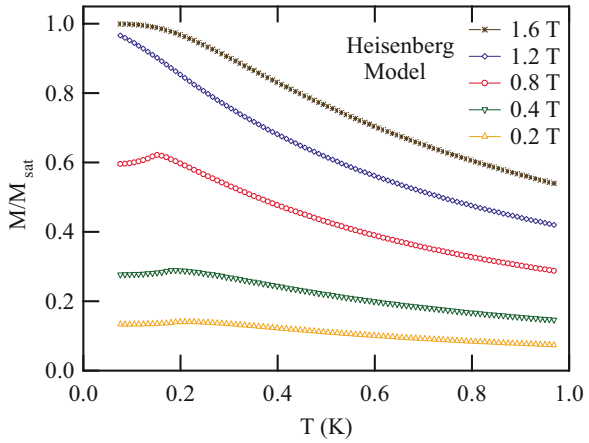

FIG. 5. (Color online) Magnetization as a function of temperature in the Heisenberg model at different applied magnetic fields.

cusp around T_N=0.18 K. It shifts to lower temperatures with field, in accord with the field evolution of the specific-heat anomaly. Together, specific-heat and magnetization measurements prove that $Ce_4Pt_{12}Sn_{25}$ undergoes an AFM phase transition at T_N=0.18 K in zero field. With magnetic field increasing above 0.6 T, the cusp feature disappears, and the magnetization is monotonic, suggesting that AFM order is suppressed in the vicinity of this field. Above 2.0 T, the magnetization develops a plateau at low temperature, as seen in Fig. 4(b). The plateau is related to the field splitting of the CEF ground-state doublet. In fact, calculations based on the CEF scheme assumed above also show similar behavior, as well as good agreement in absolute value, as indicated by a dashed curve in the inset of Fig. 4(b) obtained for 3 T using the following formula:

$$\chi = \frac{N(g_J\mu_B)^2}{Z}\left[\sum_{m\neq n}|\langle m|J_z|n\rangle|^2\frac{1-e^{E_m-E_n}}{E_m-E_n}e^{-\beta E_n} + \sum_n |\langle n|J_z|n\rangle|^2\beta e^{-\beta E_n}\right]. \quad (5)$$

The results of the Heisenberg model calculations of magnetization are displayed in Fig. 5. Similar to specific heat, the AFM transition remains very sharp and persists to higher fields within the model calculations compared to the experimental data.

Figure 6 shows isothermal magnetization curves $M(H)$ of $Ce_4Pt_{12}Sn_{25}$ at temperature of 0.1 K ($<T_N$), 0.2 K ($\approx T_N$), and 2 K ($\gg T_N$). In contrast to $M(H)$ data at 2.0 K, which increases slowly with field and does not show complete saturation up to 7 T, $M(H)$ at 0.2 K rapidly increases with field and exhibits a plateau above 2 T. The saturated value of the magnetic moment μ_s corresponds to about 0.71 μ_B/Ce, which is much smaller than the value expected for a free Ce^{3+} ion of $g_J J\mu_B$=2.14 μ_B (g_J=6/7, J=5/2). This reduction, as well as deviation of χ at low temperature, reflects CEF effects in $Ce_4Pt_{12}Sn_{25}$. Using formulas (2), (3), and (6) below, we can calculate the magnetization by using the value of B_4^0=0.5 K, the same as the one employed in calculations of the specific heat above,

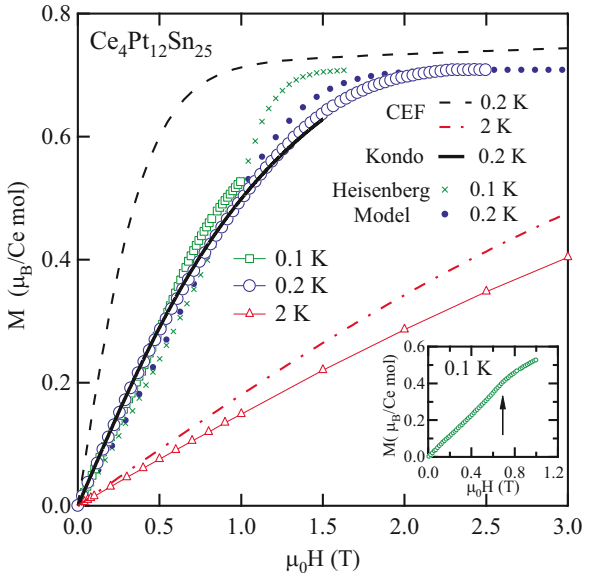

FIG. 6. (Color online) M vs H curves of $Ce_4Pt_{12}Sn_{25}$ at several temperatures of 0.1, 0.2, and 2 K. The dashed and dashed-dotted curves are obtained from the calculation at 0.2 K and 2 K, respectively, based on a CEF scheme. Solid curve is a result of the Kondo screening model described in the text. Dotted curve and crosses are numerical results based on the Heisenberg model at 0.2 K and 0.1 K, respectively. The inset shows the magnetization curve at 0.1 K. The arrow indicates the field where the data show anomaly due to antiferromagnetic ordering.

$$M = \frac{g_J\mu_B}{Z}\sum_n \langle n|J_z|n\rangle\beta e^{-\beta E_n}. \quad (6)$$

The magnetization calculated from this CEF model is also displayed in Fig. 6, for T=0.2 K (dashed line) and for T=2 K (dashed-dotted line). Agreement between the CEF model and the data is good for T=2 K$\gg J$ [similar to that in Fig. 4(b)]. As expected, there is a large discrepancy at T=0.2 K between experimental results and the calculated field dependence based on a single-ion CEF model so that only the saturated magnetic moment μ_s=0.74 μ_B/Ce is comparable to the experimental value (μ_s=0.71 μ_B/Ce). The best fit to the data at 0.2 K below 0.4 T using a Kondo screening model[34] gives T_K=1.2 K. However, this value of T_K is incompatible with specific-heat results and the analysis performed above, which indicate $T_K \leq 0.2$ K.[25] At intermediate fields the dominant physics is in the f-f interactions inherent in the Heisenberg model that we used to describe specific-heat results above. The magnetization calculated for T=0.1 and 0.2 K is also displayed in Fig. 6, and indeed reproduces the experimental data well. Small discrepancies at higher fields (calculations overestimate magnetization) that are more pronounced at low temperature, are most likely again due to a weak Kondo screening. It should be noted that at 0.1 K, below T_N in zero field, $M(H)$ shows a kink anomaly around 0.6 T, indicated by an arrow in the inset of Fig. 6. This kink corresponds to the critical field H^* where AFM order disappears, and is consistent with $C(T)/T$ and $M(T)$ in constant magnetic fields described above.

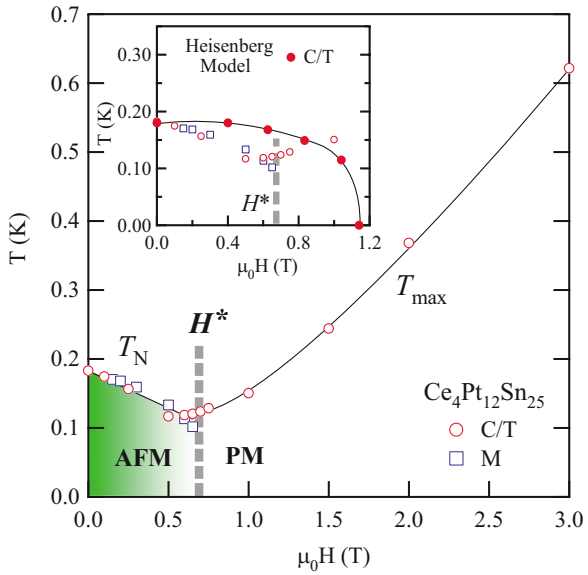

FIG. 7. (Color online) T-H phase diagram of $Ce_4Pt_{12}Sn_{25}$ deduced from specific-heat and magnetization measurements. Circle and square symbols correspond to T_{max} where $C(T)/T$ and $M(T)$ exhibit maximum, respectively. The solid curve is the eye guide. The dashed line represents the critical magnetic field H^* which could be a boundary of the ground states between AFM and PM states. Inset shows the low-field region, with results of the model calculations included.

C. H-T phase diagram

Figure 7 displays the temperature-field phase diagram of $Ce_4Pt_{12}Sn_{25}$ obtained from the data described in previous sections, with circles and squares representing T_{max} obtained from specific-heat and magnetization measurements, respectively. T_{max} ($\approx T_N$) decreases as field increases up to about 0.6 T, and T_{max} increases with further increase in magnetic field. T_N appears to vanish at a critical field $H^* \approx 0.7$ T indicated by the dashed line, where the ground state of $Ce_4Pt_{12}Sn_{25}$ changes from AFM to paramagnetic (PM). It is impossible to tell the exact manner in which T_N goes to zero from the data presented here. As illustrated in the inset, the suppression of T_N with fields is much more effective than expected from the Heisenberg model ($H^* > 1$ T). There is no divergence of Sommerfeld coefficient γ with $T \rightarrow 0$, in contrast to common behavior in materials at a QCP. Perhaps this can be explained by a small amount of entropy associated with magnetic fluctuations at high fields, as most of it is released at a higher temperature Schottky anomaly. Low-temperature spectroscopic investigations, such as NMR, μSR, or neutron scattering will be able to provide a definitive picture of how AFM order is suppressed in $Ce_4Pt_{12}Sn_{25}$.

IV. CONCLUSION

In conclusion, we have performed low-temperature field-dependent specific-heat and magnetization measurements to elucidate the ground-state properties of $Ce_4Pt_{12}Sn_{25}$. Magnetization measurements established that $Ce_4Pt_{12}Sn_{25}$ orders antiferromagnetically with a small ordering temperature $T_N = 0.18$ K in zero field, where $C(T)/T$ exhibits a huge jump of ~ 30 J/mol Ce K^2. The small value of the saturated magnetic moment of 0.71 μ_B/Ce at 0.2 K exhibited by magnetization as a function of magnetic field can be ascribed to CEF effects, with a Γ_7 ground state, as inferred from magnetic entropy. T_N is suppressed with an initial increase in field up to 0.6 T, whereas T_{max} of the maximum in $C(T)$ begins to move to higher temperature above 0.7 T. This latter evolution is ascribed to an electronic Schottky contribution from the Zeeman-split ground-state Γ_7 doublet. Therefore, it is likely that the ground state of $Ce_4Pt_{12}Sn_{25}$ changes above ≈ 0.6 T from AFM to paramagnetic. This picture is further supported by the magnetization data for both temperature and magnetic field sweeps.

The model calculations, based on a CEF scheme with a Γ_7 ground state, reproduce rather well experimental specific-heat and magnetization data in high field. Zero-field data are described very well by the numerical calculation based on the Heisenberg model. Small deviation between experimental data and numerical results may be due to frustration or Kondo screening with a low characteristic temperature $T_K \leq T_N = 0.18$ K. This indicates that electronic spins on Ce^{3+} are not screened substantially by the conduction electrons, and places $Ce_4Pt_{12}Sn_{25}$ in the $J \ll J_c$ of the Doniach phase diagram. The Kondo temperature T_K is expected to be exponentially small in this regime, and a J^2 dependence of the RKKY interaction stabilizes the AFM ground state *in spite* of a large distance between the Ce ions. $Ce_4Pt_{12}Sn_{25}$ therefore presents us with a *counter example* to an expectation that dilute f-electron compounds will likely fall into the Kondo screened regime.

Within the Heisenberg model calculations, the AFM transition is more robust to the magnetic field, compared to experimental data in low-field regime. We raised a number of questions with regard to the possible origins of this discrepancy, such as magnetic field dependence of the RKKY interaction, and frustrating effects of the next-nearest-neighbor interactions, and point to a number of fruitful future theoretical inquiries.

Further experiments will be needed to explore the details of the disappearance of the AFM state in $Ce_4Pt_{12}Sn_{25}$, as well as the origin of the long temperature tail of the specific heat above T_N, and potential role of magnetic frustration. Experiments under pressure, in particular, can help answer why T_N is so low in $Ce_4Pt_{12}Sn_{25}$ compared with other Ce compounds, as well as search for pressure-induced superconductivity, occasionally found in the vicinity of pressure-induced QCP at P_c ($T_N \rightarrow 0$).

ACKNOWLEDGMENTS

We would like to thank Hironori Sakai for useful discussions. Work at Los Alamos was performed under the auspices of the U.S. Department of Energy, Office of Basic Energy Sciences, Division of Materials Sciences and Engineering. Research at UCSD was supported by the U.S. National Science Foundation under Grant No. DMR-0802478. I.V. was supported in part by the U.S. DOE under Grant No. DE-FG02-08ER46492.

[1] J. Kondo, Prog. Theor. Phys. **32**, 37 (1964).
[2] M. A. Ruderman and C. Kittel, Phys. Rev. **96**, 99 (1954).
[3] T. Kasuya, Prog. Theor. Phys. **16**, 45 (1956).
[4] K. Yosida, Phys. Rev. **106**, 893 (1957).
[5] S. Doniach, Physica B **91**, 231 (1977).
[6] S. Doniach, in *Valence Instabilities and Related Narrow Band Phenomena*, edited by R. D. Parks (Plenum, New York, 1977), p. 169.
[7] H. v. Löhneysen, J. Phys.: Condens. Matter **8**, 9689 (1996).
[8] P. Gegenwart, J. Custers, C. Geibel, K. Neumaier, T. Tayama, K. Tenya, O. Trovarelli, and F. Steglich, Phys. Rev. Lett. **89**, 056402 (2002).
[9] A. Bianchi, R. Movshovich, I. Vekhter, P. G. Pagliuso, and J. L. Sarrao, Phys. Rev. Lett. **91**, 257001 (2003).
[10] J. Paglione, M. A. Tanatar, D. G. Hawthorn, E. Boaknin, R. W. Hill, F. Ronning, M. Sutherland, L. Taillefer, C. Petrovic, and P. C. Canfield, Phys. Rev. Lett. **91**, 246405 (2003).
[11] G. R. Stewart, Rev. Mod. Phys. **73**, 797 (2001).
[12] G. R. Stewart, Rev. Mod. Phys. **78**, 743 (2006).
[13] P. A. Lee, T. M. Rice, J. W. Serene, L. J. Sham, and J. W. Wilkins, in *Comments on Condensed Matter Physics* (Gordon and Breach, Science Publishers, London, UK 1986), Vol. XII, p. 99–161.
[14] P. Sinjukow and W. Nolting, Phys. Rev. B **65**, 212303 (2002).
[15] J. R. Iglesias, C. Lacroix, and B. Coqblin, Phys. Rev. B **56**, 11820 (1997).
[16] T. Rappoport and M. Continentino, J. Phys. A **34**, 10829 (2001).
[17] A. L. Cornelius and J. S. Schilling, Phys. Rev. B **49**, 3955 (1994).
[18] Y.-F. Yang, Z. Fisk, H.-O. Lee, J. D. Thompson, and D. Pines, Nature (London) **454**, 611 (2008).
[19] H. Sugawara, S. Osaki, M. Kobayashi, T. Namiki, S. R. Saha, Y. Aoki, and H. Sato, Phys. Rev. B **71**, 125127 (2005); N. Kurita, M. Hedo, M. Koeda, M. Kobayashi, H. Sato, H. Sugawara, and Y. Uwatoko, *ibid.* **79**, 014441 (2009), and references therein.
[20] M. S. Torikachvili, S. Jia, E. D. Mun, S. T. Hannahs, R. C. Black, W. K. Neils, D. Martien, S. L. Bud'ko, and P. C. Canfield, Proc. Natl. Acad. Sci. U.S.A. **104**, 9960 (2007).
[21] S. Jia, N. Ni, G. D. Samolyuk, A. Safa-Sefat, K. Dennis, H. Ko, and G. J. Miller, S. L. Bud'ko, and P. C. Canfield, Phys. Rev. B **77**, 104408 (2008).
[22] Y. Saiga, K. Matsubayashi, T. Fujiwara, M. Kosaka, S. Katano, M. Hedo, T. Matsumoto, and Y. Uwatoko, J. Phys. Soc. Jpn. **77**, 053710 (2008).
[23] E. D. Bauer, C. Wang, V. R. Fanelli, J. M. Lawrence, E. A. Goremychkin, N. R. de Souza, F. Ronning, J. D. Thompson, A. V. Silhanek, V. Vildosola, A. M. Lobos, A. A. Aligia, S. Bobev, and J. L. Sarrao, Phys. Rev. B **78**, 115120 (2008).
[24] B. Chafik El Idrissi, G. Venturini, and B. Malaman, Mater. Res. Bull. **25**, 807 (1990).
[25] H.-O. Lee, N. Kurita, P.-C. Ho, C. L. Condron, P. Klavins, S. M. Kauzlarich, M. B. Maple, R. Movshovich, J. D. Thompson, and Z. Fisk, J. Phys.: Condens. Matter **22**, 065601 (2010).
[26] T. Sakakibara, H. Mitamura, T. Tayama, and H. Amitsuka, Jpn. J. Appl. Phys., Part 1 **33**, 5067 (1994).
[27] M. S. Kim, M. C. Bennett, and M. C. Aronson, Phys. Rev. B **77**, 144425 (2008).
[28] H. v. Löhneysen, T. Pietrus, G. Portisch, H. G. Schlager, A. Schröder, M. Sieck, and T. Trappmann, Phys. Rev. Lett. **72**, 3262 (1994).
[29] C. D. Bredl, S. Horn, F. Steglich, B. Lüthi, and R. M. Martin, Phys. Rev. Lett. **52**, 1982 (1984).
[30] H.-U. Desgranges and K. D. Schotte, Phys. Lett. **91A**, 240 (1982).
[31] Lack of four-fold symmetry in a cubic CEF configuration, as in $Ce_4Pt_{12}Sn_{25}$, gives rise to the sixth CEF terms in addition to a formula (2) for O_h. See, K. Takegahara, H. Harima, and A. Yanase, J. Phys. Soc. Jpn. **70**, 1190 (2001). For the purpose in this study, neglecting the sixth CEF terms does not affect the discussion.
[32] K. W. H. Stevens, Proc. Phys. Soc., London, Sect. A **65**, 209 (1952).
[33] M. T. Hutchings, in *Solid State Physics: Advances in Research and Applications*, edited by F. Seitz and B. Turnbull (Academic, New York, 1965), Vol. 16, p. 227.
[34] K. D. Schotte and U. Shotte, Phys. Lett. **55A**, 38 (1975).